Insights into the Impact of Temperature on the Wettability Alteration by Low Salinity in Carbonate Rocks

Mahani, H; Menezes, R.; Berg, S.; Fadili, Ali; Nasralla, R.; Voskov, D.; Joekar-Niasar, V

DOI
10.1021/acs.energyfuels.7b00776

Publication date
2017

Document Version
Final published version

Published in
Energy & Fuels

energy&fuels

Article

pubs.acs.org/EF

Insights into the Impact of Temperature on the Wettability Alteration by Low Salinity in Carbonate Rocks

H. Mahani,*[,†] R. Menezes,[‡] S. Berg,[†] A. Fadili,[†] R. Nasralla,[†] D. Voskov,[‡] and V. Joekar-Niasar[§]

[†]Shell Global Solutions International B.V., 2288 GS Rijswijk, The Netherlands

[‡]Delft University of Technology, 2628 CN Delft, The Netherlands

[§]The University of Manchester, Manchester, United Kingdom, M13 9PL

Supporting Information

ABSTRACT: It has been proposed that increased oil recovery in carbonates by modification of ionic composition or altering salinity occurs mainly at a temperature exceeding 70−80 °C. The argument was that elevated temperatures enhance adsorption of the potential determining ions which then modifies wettability to a less-oil-wetting state. According to this rationale, it becomes questionable if diluted brines or brines without these ions can be still applicable. Therefore, the aim of this paper is to investigate if the wettability alteration truly depends on temperature and if so how the trend with temperature can be explained. We followed a combined experimental and theoretical modeling approach. The effect of brine composition and temperature on carbonate wettability was probed by monitoring contact angle change of sessile oil droplets upon switching from high salinity to lower salinity brines. IFT measurements as a function of salinity and temperature along with extensive ζ-potential measurements as a function of salinity, pH, temperature, and rock type were conducted. Interaction potentials between oil and carbonate surfaces were estimated based on DLVO theory, and its consistency with oil-droplet data was checked to draw conclusions on plausible mechanisms. Three carbonate rocks (two limestones and one dolomite) were used along with two reservoir crude oils, high salinity formation water (FW), seawater (SW), and 25 times diluted seawater (25dSW) as low salinity (LS) brine. It was observed that (i) wettability alteration to a less-oil-wetting state can occur at ambient temperature for specific rock types and brines, and (ii) there is no univocal increase in response to SW and LS brine at elevated temperature. The largest improvement in wettability was observed for dolomite, while, among the limestones, only one rock type showed noticeable wettability improvement at elevated temperature with SW. The difference in behavior between limestones and dolomite indicates that the response to brine composition change depends on rock type and mineralogy of the sample. These observations are consistent with the ζ-potential trends with salinity at a given temperature. Dolomite generally shows more positive ζ-potential than limestones. However, even the two limestones react differently to lowering salinity and exhibit different magnitude of ζ-potential. Moreover, it is observed that, at a specific salinity, an increase in temperature leads to reduction of ζ-potential magnitude on both rock/brine and oil/brine interfaces toward zero potential. This can affect positively or negatively the degree of wettability alteration (to a less-oil-wetting state) at elevated temperature depending on the sign of oil/brine and rock/brine ζ-potential in SW/LS. The observed trends are reflected in the DLVO calculations which show consistency with contact angle trends with temperature and salinity. According to the DLVO calculation, the lack of response to SW/LS in some of the systems above can be explained by stronger electrostatic attractive forces under SW/LS than HS. This study concludes that a combined surface-charge change and double-layer expansion is a plausible mechanism for the wettability alteration in carbonate rocks.

INTRODUCTION

Low salinity waterflooding (LSF) is an improved/enhanced oil recovery method which has been widely researched within the past decade. This method is similar to a conventional waterflood but involves injecting brine with modified composition associated with an overall lower salt content (as compared to the existing formation waters in the media) into the reservoir to increase the oil recovery. LSF in this context does not necessarily refer to usage of low salinity brines, rather to the technology in which either brine composition is modified or salinity is reduced to produce incremental oil recovery. Different institutions or companies use other terms, but all refer to basically same technology.

The introduction of LSF in an equilibrium crude oil−rock−brine system with high salinity formation water appears to cause a shift to a new system equilibrium which tends to favor improved oil recovery. LSF is a multilength scale process, covering the interactions at molecular scale up to core scale and beyond. Manifestation of low salinity effect (LSE) at core scale is an increase or acceleration of oil recovery relative to high salinity at a given water-cut or pore-volume injected. At pore-network scale, the LSE is manifested as an improvement in the microscopic displacement efficiency. At sub-pore scale (or mineral surface), most studies in the literature suggest that LSE is a wettability alteration from a more-oil-wetting state toward a more water-wetting state (see, for instance, refs 2−4 for sandstones and refs 5−11 for carbonates). Nevertheless, as demonstrated in ref 1, the occurrence of wettability alteration at sub-pore scale (which is probed as contact angle change) does not necessarily translate into incremental oil recovery at core

Received: March 17, 2017
Revised: July 4, 2017
Published: July 6, 2017

DOI: 10.1021/acs.energyfuels.7b00776
Energy Fuels 2017, 31, 7839−7853

Table 1. Bulk Mineral Composition for Each Rock Type (in wt %) Using XRD Analyses

rock sample	kaolinite	K feldspar	quartz	plagioclase	calcite	dolomite
Limestone A	0	0	trace	0	100	0
Limestone B	0	0	1	0	99	0
Dolomite	0	0	1	0	0	99

scale; in other words, other processes occurring between the sub-pore and core scale should work optimally to facilitate oil release, mobilization, transport in the pore network, banking, and eventually production. Another aspect in understanding the LSF process is that wettability alteration is a consequence rather than a cause, and the underlying microscopic mechanisms are still debated. The main challenge toward understanding the mechanisms is that the evidence is often indirect and has been inferred mainly from experiments at core scale.

Various studies on carbonates (see, for instance, refs 2, 6−12) have demonstrated a positive effect of salinity reduction on oil recovery in a wide range of salinity from below 1000 ppm to 45000 ppm (close to seawater salinity) or even higher (albeit, still lower than formation water salinity). Several studies including the ones performed by the Austad group[13,14] suggested that not only lowering salinity but modifying the brine composition more specifically could also lead to IOR in carbonate rock. This has been attributed to the effect of potential determining ions (PDIs) such as SO_4^{2-}, Ca^{2+}, and Mg^{2+} which are present in brines like seawater, which is a major source for waterflooding projects.

Some researchers have also hypothesized that the increase in oil recovery could be caused by carbonate mineral dissolution.[15] However, the experiments under equilibrium conditions suggested to rank the mineral dissolution as a secondary mechanism, not a primary one.[16,17] Researches by refs 18 and 19 highlighted the effect of PDIs, particularly SO_4^{2-}, on the change of surface charge of calcite toward a more water-wetting state. Recent studies by Mahani et al.[17,20] showed a consistency between ζ-potential trends with salinity, oil-droplet experiments, and core scale experiments, suggesting surface-charge alteration in combination with expansion of the electric double layer to be a plausible mechanism for the wettability alteration in carbonates.

In particular, in the case of carbonate rock, previous studies have shown that the effect of LSF in carbonates is temperature-dependent (see refs 5, 14, 15, 19, 21−26). Austad and co-workers[5,19,23−25] have conducted several studies to show the effect of temperature toward the specific individual PDIs which preferentially adsorb onto the carbonate surface at elevated temperatures. This has led to the view that LSF in carbonate is applicable mainly at elevated temperatures which would influence the screening criteria for reservoirs (which are usually at high temperature, i.e., >60 °C). In addition, with diluted brines or brines without the PDIs such as pure NaCl brine, that becomes questionable if still LSE can be observed, which would have a major consequence for field applications and laboratory level screening studies.

Therefore, the aim of this paper is to investigate if the LSE truly depends on temperature and if so how the trend with temperature can be explained. As mentioned above, since wettability alteration is the most agreed upon effect of low salinity, we consider this particular process/aspect as the general framework of our study.

Most of the previous studies on LSF in carbonates have been conducted at the core/Darcy scale, which usually provides quantitative analysis on the incremental recovery obtained by LSF. This scale averages over such a large volume of rock and a wide range of heterogeneities, which makes core scale data difficult to use in concluding on what is the exact mechanism behind the LSE in carbonates. Hence, in order to understand the driving mechanisms and the effect of temperature, we need to study the molecular interactions and surface energies between the crude oil−rock−brine (COBR) interfaces at the sub-pore level. This will further help us to attain consistency of the LSE between the sub-pore to core scale. For achieving that, we design a set of experiments coupled with a modeling approach to validate our results.

The experimental work is categorized under two subscales: (i) the macroscopic scale where we can actually visualize the wettability alteration process by measuring contact angle changes at elevated temperatures, and (ii) the surface scale where the electric potential at oil/brine and rock/brine interfaces are quantified via ζ-potential measurements as a function of salinity, pH and temperature. Further oil/brine interfacial tension (IFT) measurements are performed at elevated temperatures to study the liquid-liquid surface energies.

We use a DLVO (Derjaguin, Landau, Verwey, and Overbeek) model to estimate the interaction potential between the oil and rock interfaces under LS and and high salinity (HS) conditions and its trend with temperature. The measured ζ-potentials at respective salinity and pH are used as inputs to this model.

MATERIALS, METHODS, AND PROCEDURES

Carbonate Rocks. To investigate the influence of rock, two types of carbonate materials were used: limestone and Silurian dolomite. The limestone materials were taken from 2 different Middle Eastern reservoirs and are referred to as Limestone A and Limestone B in this study and the dolomite sample was taken from the Silurian dolomite outcrop. Prior to the experiments, the limestone samples were cleaned using a Soxhlet apparatus first with refluxing toluene, followed by an azeotropic mixture of chloroform/methanol/water. The cleaned samples were dried in a vacuum oven at 95 °C. On the dolomite outcrop sample, no cleaning was performed.

The mineral compositions estimated from X-ray diffraction (XRD) of the samples are presented in Table 1. The materials contain negligible amounts of clay.

The carbonate materials were initially crushed to a powder (size < 45 μm) before observation under XRD. This helps us replicate the size of the material being used during the experimental study.

Brines. Synthetic brines were used in the study. The brines were prepared by mixing deionized water and varying amounts of pure salts (Merck grade): NaCl, $MgCl_2{\cdot}6H_2O$, $CaCl_2{\cdot}2H_2O$, KCl, $SrCl_2{\cdot}6H_2O$, Na_2SO_4, $NaHCO_3$. Formation brines (FW_A and FW_B) compositions were taken from the same Middle Eastern reservoirs as the limestone samples. Further, seawater (SW) and 25 times diluted seawater (25dSW) as LS brine were used. The brines were allowed to equilibrate for a few hours, after which they were heated to 80−100 °C for 3−4 h. They were further filtered through a 1.2 μm filter (Millipore) to avoid the effect of excessive precipitation while conducting the experiments at elevated temperatures. The brine pH

DOI: 10.1021/acs.energyfuels.7b00776
Energy Fuels 2017, 31, 7839−7853

Table 2. Brine Compositions for Various Brines Used in the Study

ion	FW_A (mg/L)	FW_B (mg/L)	SW (mg/L)	25dSW (mg/L)
Na^+	49 898	77 203	13 404	536
K^+	0	1881	483	19
Mg^{2+}	3248	1819	1618	65
Ca^{2+}	14 501	11 651	508	20
Sr^{2+}	0	0	17	1
Cl^-	111 812	146 321	24 141	967
SO_4^{2-}	234	369	3384	135
HCO_3^-	162	150	176	7
TDS	179 855	239 394	43 731	1751
ionic strength (mol/L)	3.659	4.50	0.869	0.035
pH	6.9	7	7.8	7.5

Table 3. Chemical and Physical Properties of Crude Oils

oil sample	acid number (mg KOH/g)	base number (mg KOH/g)	asphaltene (g/100 mL)	density (g/cm^3) at 20 °C	viscosity (cP) at 20 °C
Crude A	0.5	1.0	0.244	0.865	20.7
Crude B	0.39	1.84	12.37	0.93	179.2

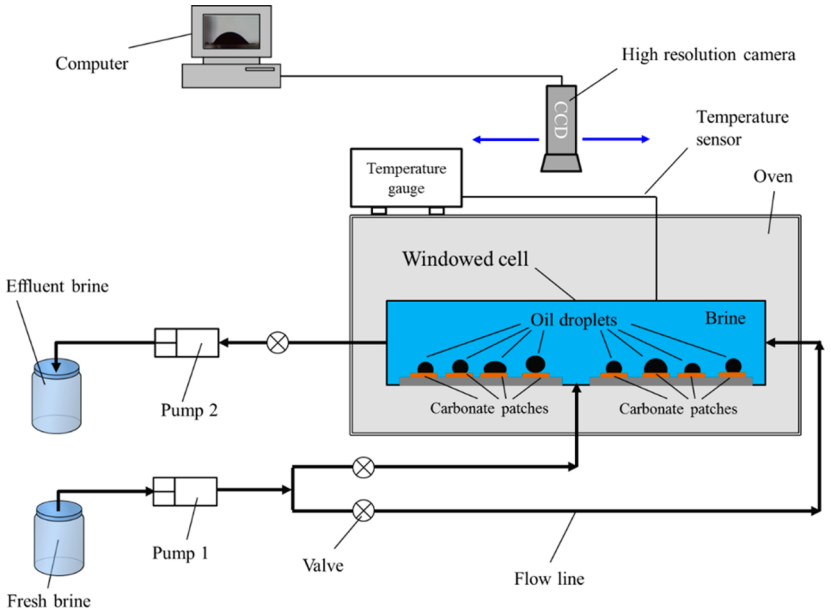

Figure 1. Schematic of the oil-droplet experimental setup under elevated temperature (HT). Note that the oven has a glass window for visualization. The camera is placed outside the oven and looks through the window. The camera is moved horizontally to acquire 10−15 droplets in one experiment simultaneously to provide sufficient statistics.

and conductivity were measured before and after filtration to account for any change in the brine properties. The brine compositions are given in Table 2.

Crude Oil. Two types of crude oils (Crude A and Crude B) were used, which were taken from the same Middle Eastern carbonate reservoirs as the limestone samples; i.e., the crude oil matches the reservoir rock. The oil was centrifuged and filtered through a 1.2 μm filter (Millipore) and subsequently analyzed for physical and chemical properties as given in Table 3. Crude A was used for experiments with both Limestone A and Dolomite samples. Respectively, Crude B was used for experiments with Limestone B.

Oil-Droplet (Contact Angle) Experiments at Elevated Temperatures. The oil-droplet experiments aimed at measuring contact angle changes for different rock samples as a function of temperature and brine composition. Each experiment was performed over a duration of roughly 2 weeks. The details of the setup and experimental protocol are given below.

Visual observation of wettability alteration in terms of contact angle change at elevated temperatures has not been reported in the literature very extensively. Some studies have tried to capture this effect through contact angle measurements based on a pendant drop approach, which uses a tilted rock surface to measure advancing/receding contact angles.[21] From previous experience, oil droplets in that geometry (i.e., pendant drop) are separated from the rock by a thick water film without actual binding of oil to the mineral surface, which is not representative for the situation in the reservoir. It has been observed that, if the rock surface is tilted (or further tilted), the oil droplet moves freely on the surface. Our study uses a unique method of creating sessile oil droplets on a model rock surface (carbonate patch), which follows from previous studies on sandstones using clay patches[27,28] and carbonate rocks.[17] The model system is first exposed and equilibrated with HS brine and then exposed to SW and LS brines. Here, we concentrate on *changes* to contact angle upon salinity change, rather than the absolute magnitude of the contact angle—as done in most studies (see, e.g., ref 5). Each experiment ran for approximately 160−260 h.

To perform oil-droplet experiments, a built for purpose setup was utilized to perform high temperature/high pressure (HT/HP)

DOI: 10.1021/acs.energyfuels.7b00776
Energy Fuels 2017, 31, 7839−7853

experiments which allows us to monitor contact angles of dozens of oil droplets at the same time (refer to Figure 1 for the entire setup and the flow infrastructure). This possibility improves statistics and enables observing the contact angle trends better than the common practice of monitoring only one droplet at a time.

The experiments were performed on a model carbonate substrate (see the section Preparation of Carbonate Substrate) made by depositing thin carbonate layers (referred to as patches) on microscope slides; onto these rock patches, oil drops (approximately 3.8−4 μL) were placed with a calibrated pipet. The slides were transferred onto a steel plate that accommodates 2 slides, each of which contains 5−6 carbonates patches; the assembly was placed inside a glass windowed cell and shut from outside air exposure. The cell was then mounted onto a steel frame inside the oven and connected to the brine inlet and outlet lines. The oven was then heated to the required temperature. The windowed cell has been designed to withstand pressure and temperature up to 34 bar and 160 °C, respectively.

The brines were then pumped and retracted from the cell using two Quizix pumps at a constant maximum flow rate of 7.5 mL/min. The initial brine used to fill the cell (cell total volume 100 mL) is HS formation water (FW) in order to establish a baseline for contact angle comparison between HS FW and the subsequent SW/LS condition. The safety pressure used while operating the pumps is 8 bar to avoid over pressurizing the cell, which might affect the oil drop formation. The oil drops were allowed to rest under a "no flow" condition for approximately 24−48 h (the equilibration step) under HS until no further contact angle change is observed.

Real-time images were captured every 2−4 h from each individual droplet to monitor any change to the contact angle. To acquire the images, a NIKKOR 105 mm lens combined with an Imaging Source 72 series CMOS camera was used. The horizontal motion of the camera was automated using the LabView software where x−y positions of the individual oil droplets were registered at the beginning of the experiment.

After equilibration under HS condition, the brine change was made by switching on the Quizix pump (filled beforehand with SW/LS brine) and flowing for a period of approximately 3 h or 1000 mL of SW/LS brine. Before and after performing a brine change, a sample of the retracted brine from the cell and the new brine pumped was taken to measure the pH and conductivity, which helps us verify that the brine change was done completely and the entire cell was fully flushed with the new brine. Once assured that the cell was entirely flushed with the SW/LS brine, we stop the flow and observe the contact angle changes over a period of time (under no flow - static conditions). It is noteworthy to mention that the oil droplets were not affected during the flow period. A flat panel light source was placed inside the oven to illuminate the oil droplets from the back, which allows us to obtain high quality images for contact angle analysis. This entire setup had to be free from any disturbance and shock vibrations during an experiment. For this reason, the whole setup was mounted on a vibration absorbing breadboard.

Preparation of Carbonate Substrate. The carbonate rock surface was represented by carbonate patches made from crushed rock suspension in demineralized water, following a procedure previously described in ref 17. A microscopic slide was thoroughly cleaned using Hellmanex detergent. Thereafter, the slide was rinsed with demineralized water and then dried with nitrogen. The next step was to use a motorized pipet to create 2−4 μm thick circular patches using the supernatant part of the suspension (approximately 4 μL) per patch. The slides were then allowed to dry in a desiccator under vacuum for 45 min. Once the slides were removed from the desiccator, the rock surface deposited on it would stick naturally to the slide due to the water wetness. Further, oil drops were deposited over each patch (approximately 3.8−4 μL) and then transferred to the windowed cell to conduct the experiments. When oil is applied on the dried patch, it spreads over the whole patch. In the next step, when oil-carbonate is exposed to formation brine, the oil droplet is formed due to recession of the three-phase contact line as a result of the balance between buoyancy and adhesion forces.

Contact Angle Measurement. The contact angle was measured as a function of exposure time to different brines under static condition. The high-resolution images were analyzed using the DSA100 software from KRÜSS GmbH to determine the macroscopic contact angle of the oil droplets through the denser brine phase. The contact angle was determined by fitting a contour to the oil droplet, and selecting a baseline at the solid surface onto which the oil droplet sits. Further, a tangent to the contour was determined and the arithmetic average of the left and right contact angles was recorded.

Errors in the measurement were relatively small (±2°) due to high quality of the produced images. The errors mainly occur at the first moment after a brine change or at a temperature change due to transition of brine refractive index from high salinity to low salinity condition. This results in a noticeable shift of the image of the droplets projected on the camera which could cause an error while determining the baseline.

ζ-Potential Measurement. The ζ-potential was measured using a Zetasizer Nano-ZS (Malvern Instruments). The instrument measures the electrophoretic mobility of particles within a suspension of rock particles or oil droplets dispersed in a respective brine. Further, the ζ-potential is obtained from the electrophoretic mobility using the Smoluchowski approximation of Henry's equation.[29] This setup allowed measurement up to a maximum temperature of 70 °C at ambient pressure. To capture the effect of temperature on brine viscosity in the ζ-potential estimation using Henry's equation, brine viscosity at the measurement temperature is inputted to the Zetasizer software.

Carbonate rock/brine suspensions were prepared following the same approach used in our previous study,[20] by mixing 0.2 g of crushed carbonate rock particles (size < 45 μm) with 20 mL of prepared brine, which accounts for 1% weight of the aqueous solution. The supernatant part of the suspension was used for the ζ-potential measurement.

For oil/brine ζ-potential measurement, a new approach as compared to the previous studies was followed which provided more stable emulsion and higher quality results. Initially, an oil/brine emulsion was prepared by using a 1:20 volume ratio (1 mL of crude oil with 20 mL of brine) which was kept in a sweep-enabled sonicator bath for 45 min. This provided a coffee colored, opaque oil-brine emulsion. This emulsion was left to rest for a day to equilibrate. Prior to performing measurements, a volume between 2 and 4 mL of the original emulsion was diluted (mixed) with 10 mL of brine (i.e., the same brine used to prepare the original emulsion) to produce a more dispersed and transparent emulsion. This ratio was decided after performing ζ-potential screening tests with varying concentrations of emulsion and brine, to finally obtain the optimum ratio which provided more stable measurements, thus more consistent results with good repeatability.

The rock/brine and oil/brine suspensions were allowed to equilibrate for a day before the measurements were performed. The pH of the suspension was adjusted by manually adding drops of concentrated hydrochloric acid (HCl) and/or sodium hydroxide (NaOH) solutions. The mixture was stirred and allowed to rest for 15−20 min until the pH value stabilized.

Rock/brine ζ-potential measurements were performed between a pH range of 6−10, below and above which the dissolution of carbonate and precipitation, respectively, led to unstable measurements. We were particularly interested in pH values exceeding 7.5−8.0, because carbonates dissolve in under-saturated LS brine, which results in a pH increase to 8.5−9.0. For oil/brine ζ-potential, the measurement was performed over a wider pH range (4−10) because the samples were quite stable as compared to the rock samples which were affected by the buffering effect of dissolution. The measurements at lower pH values were mainly conducted to capture the IEP.

The average value of 3−5 measurements with 15−100 runs each was recorded as the ζ-potential value, along with an error bar based on the standard deviation of the repeated measurements. The measurements for each sample (rock and oil) were conducted at 3 temperatures (25, 50, 70 °C). To improve the quality of measurements at higher temperatures, the electrode cells containing the

DOI: 10.1021/acs.energyfuels.7b00776
Energy Fuels 2017, 31, 7839−7853

suspensions were flushed after every 1−2 measurements with a fresh sample. This could be monitored by observing a fairly constant conductivity value at that respective temperature.

DLVO Interaction Force Calculation. Interfacial forces acting between the rock and oil surfaces present in a brine medium were estimated using DLVO theory.[30] The interaction forces between the two surfaces separated at distance "h" (representing water film thickness) is related to the free energy of two surfaces $W(h)$ per unit area. The free energy "W" is the summation of van der Waals (VDW), electrical double layer (EDL), and structural (S) free energies as a function of "h".

$$W(h) = W_{VDW}(h) + W_{EDL}(h) + W_S(h) \quad (1)$$

The derivative of these (interaction) energies per unit area with respect to the separation distance (h) in the direction normal to that of the interacting surfaces is known as the disjoining pressure (Π):

$$\Pi = -\frac{\partial(W_{VDW} + W_{EDL} + W_S)}{\partial h} \quad (2)$$

A positive interaction energy (potential) which corresponds to a positive disjoining pressure would relate to a repulsive force between the rock and oil surfaces. The more negative the net interaction potential value, the more attractive the forces get between the charged surface. This would mean a less-oil-wetting (or more water-wetting) system for a positive interaction potential and more oil-wetting (less water-wet) for a negative interaction potential, respectively.

The van der Waals force dominates when the separation between the surfaces (h) is small (few nanometers). It is also rather insensitive to the concentration of the electrolytes. However, they are very important to consider while looking at high salinity brines due to the compressed film and smaller thickness (h). On the other hand, the electrostatic double-layer repulsion is strong at larger separations (10's of nanometers), and it is quite sensitive to the concentration of electrolytes, especially at lower salt levels. Although there are other non-DLVO forces like hydration/structural forces that could play an important role at very small separation distances, we neglect them in our study as they are valid only below the range of 1 nm. Hence, we calculate the DLVO interaction energy (potential) based only on the VDW and EDL contributions.

The VDW forces are usually present and originate due to the dipole-dipole, dipole-induced-dipole, and dispersion forces. A widely used simple approximation based on the Lifshitz theory to calculate the van der Waals interaction energy (W_{VDW}) is given by

$$W_{VDW} = -\frac{A}{12\pi h^2} \quad (3)$$

where "A" is the Hamaker constant which defines the strength of the VDW force and is a function of the dielectric permittivities of the media, in our case rock (ε_s), brine/water (ε_w), and crude oil (ε_o) which varies mainly with temperature:

$$A = \frac{3}{4}k_B T\left(\frac{\varepsilon_o - \varepsilon_w}{\varepsilon_o + \varepsilon_w}\right)\cdot\left(\frac{\varepsilon_s - \varepsilon_w}{\varepsilon_s + \varepsilon_w}\right) \quad (4)$$

In this equation, k_B is the Boltzmann constant and T is the temperature in (K). The typical values for the Hamaker constant are within the range of (10^{-21} to 10^{-19} J). On the basis of the permittivity values of the COBR system studied here (refer to Table A-1), the Hamaker constant is positive because $\varepsilon_o < \varepsilon_s < \varepsilon_w$; thus, the VDW forces are attractive.

The EDL forces are caused by the potentials at the surfaces which are quantified via the ζ-potential. The EDL free energy can be obtained from solution of the Poisson−Boltzmann equation (PBE), which, in one-dimensional form, can be expressed as

$$\frac{d^2\Psi}{dh^2} = \frac{-e}{\varepsilon_w\varepsilon}\sum z_i\rho_i \exp\left(\frac{-z_i e\Psi}{K_B T}\right) \quad (5)$$

where Ψ is the electrostatic potential, ε is the permittivity of vacuum, and e is the charge of a proton (1.6×10^{-19} Coulomb). z_i and ρ_i are the valency and charge density of different ions (i), respectively, used for complex electrolyte solutions.

The summation in eq 5 accounts for electrolytes containing a mixture of ions with varying valences. In our case, the 2 charged surfaces (rock and oil) can be treated as charged flat plates surrounded by brine.

As seen from eq 5, the PBE is a nonlinear, second-order differential equation and is nontrivial to solve for electrostatic potential directly. The true solution for the interaction potential and in-turn the disjoining pressure is obtained by solving the full PBE; however, to estimate the forces as a function of salinity and temperature, we have used the Debye−Hückel (D-H) approximation to obtain the linearized solution for the EDL forces. The D-H approximation holds for $\left(\frac{z_i e\Psi}{K_B T}\right) < 1$, or in terms of the potential, it is valid for systems having low surface charges with potentials approximately less than 25 mV at 25 °C.[31] For our nonhighly charged system, which is reflected through the ζ-potential measurements, this condition is usually met, although, for crude/brine, the ζ-potential in 25dSW (as will be shown later) is slightly < −25 mV, which can make the approximation less valid.

The analytical solution can be obtained for two types of boundary conditions: (i) CP-CP and (ii) CC-CC. The CP-CP boundary condition assumes constant potential (CP) on both oil and rock interfaces, whereas the CC-CC boundary condition assumes constant charge (CC) on both interfaces. The CP-CP boundary condition provides at times an underestimation (the lower limit) of the electrostatic potential[32] that can be obtained between the two interfaces. The low electrical potential under this boundary condition occurs due to charge regulation on the surface with a lower potential when two charged interfaces approach each other. Conversely, under CC-CC condition, when two charged interfaces approach each other, the potential between the surfaces varies while the surface-charge density remains constant due to restricted charge regulation. This condition provides an overestimation (i.e., the upper limit) of the true electrostatic potential between the two interfaces.[32] This is due to the fact that, when two interfaces with fixed charges approach each other, the overall charge density in the film region increases, producing a net repulsive interaction potential or force.

For the COBR system, the true boundary condition seems to be closer to CC on the oil and CP on the rock interface as suggested in some studies (for instance, ref 33). However, there is no general analytical solution in this case and it has to be obtained numerically. It is known that the CC-CC condition predicts extremely large repulsive forces as compared to the constant potential (CP-CP). In this work, we decided to estimate the forces as simple and realistic as possible using an analytical solution. That is why we focus on an analytical solution for CP-CP condition and neglect CC-CC.

On the basis of the analytical solution of linearized PBE under CP-CP boundary condition, the EDL interaction energy (potential) can be derived as follows[30,34]

$$W_{EDL}(h) = \frac{\varepsilon\varepsilon_w k[2\zeta_1\zeta_2 - (\zeta_1^2 + \zeta_2^2)e^{(-kh)}]}{2\sinh(kh)} \quad (6)$$

where ζ_1 and ζ_2 are the ζ-potentials on the rock/brine and oil/brine interfaces, respectively; k is the inverse of the Debye length

$$k^{-1} = \sqrt{\frac{\varepsilon\varepsilon_0 K_B T}{2N_A e^2 I}} \quad (7)$$

wherein $I = 0.5\sum z_i^2\rho_i$ or the ionic strength.

Interfacial Tension (IFT) Measurements. Oil-brine IFT measurements were conducted using an HT/HP tensiometer setup DSA100 from KRÜSS GmbH. Crude B IFT in different brines were measured at temperatures ranging from 25 to 100 °C and pressures of 1−5 bar corresponding to the pressures maintained during the oil-droplet experiments. Crude A IFT with FW_A and 25dSW was measured mainly at 25 °C—a higher temperature was not attempted. Crude A IFT in SW was measured at both 25 and 80 °C.

DOI: 10.1021/acs.energyfuels.7b00776
Energy Fuels 2017, 31, 7839−7853

A standard pendant drop approach was followed to calculate IFT via fitting the Young−Laplace equation to the oil-droplet profile. Equilibrium was reached after approximately 2000 s, during which we observe a decline in the IFT toward a steady value. This steady value was recorded as the expected (true) IFT value; 3−5 measurements at each temperature were performed for each oil/brine system for reproducibility. During measurement, no precipitation was observed at the oil/brine interface particularly in FW; thus, no effect on IFT trend with temperature is expected. The IFT error is ±1 mN/m.

RESULTS AND DISCUSSION

In this study, the main parameter used to evaluate the influence of brine salinity and temperature on wettability alteration is contact angle change; therefore, we would first like to present the measured contact angle data for each rock type at ambient (25 °C) and reservoir temperatures (80 °C for Limestone A and Dolomite and 100 °C for Limestone B) using two brines (i.e., SW and 25dSW). To validate our observations, we then present the ζ-potential data which are used to further build our DLVO model. These experiments would complement some previous coreflooding results (see ref 12) and help to understand the consistency of the LSF mechanism at various length scales from pore to core/Darcy scales.

Effect of Temperature and Rock Type on the Low Salinity Effect. Before we delve into the results for each rock separately, we first give a summary of the contact angle change observed for all the experiments performed using SW and 25dSW at different temperatures. The contact angle change ($\Delta\theta$) is the difference between the contact angle of a droplet at the time of equilibration with FW and at the end of exposure to SW or 25dSW. Figure 2 illustrates the overall impact of temperature for each rock. Each point in the plot represents the result of one oil droplet (either in SW or in 25dSW), and the horizontal black bars indicate the average value at a particular temperature for each respective rock.

From Figure 2, we can conclude that a temperature increase can indeed increase the change in contact angle ($\Delta\theta$) or improve the LSE toward a less-oil-wetting state, but it depends on the rock type. In particular rock types, we see the increase, whereas, in some rock types, we observe a similar contact angle change at both (25 and 100 °C) temperature ranges. Limestone A shows an LSE at 25 °C as well as at 80 °C, while Limestone B shows a slightly improved LSE at elevated temperature (100 °C). Dolomite shows minor change at ambient temperature for both the brine types but at elevated temperatures (80 °C) shows a relatively large change in contact angle, toward a less-oil-wetting state that would subsequently lead to incremental oil recovery. Overall, this is an important observation as previous studies (see, e.g., refs 19, 23−26) looking at the specific effect of PDIs led to the belief that LSF can mainly change wettability and increase recovery at reservoir (elevated) temperatures, which is not the case.

It is worth mentioning that the wide range of contact angle changes observed within each rock type is mainly due to the surface roughness of the carbonate patches (as no two patches are identical), creating "pinning points" or "asperities", which affect the recession of the three-phase contact line and result in different initial contact angles. The method produces oil droplets with somewhat oil-wet to intermediate-wet initial condition as suggested as an appropriate/relevant initial condition in carbonate (see, e.g., ref 9). What is more important is the consistency of the observation for several of the droplets, which then gives confidence that the LSE is robust

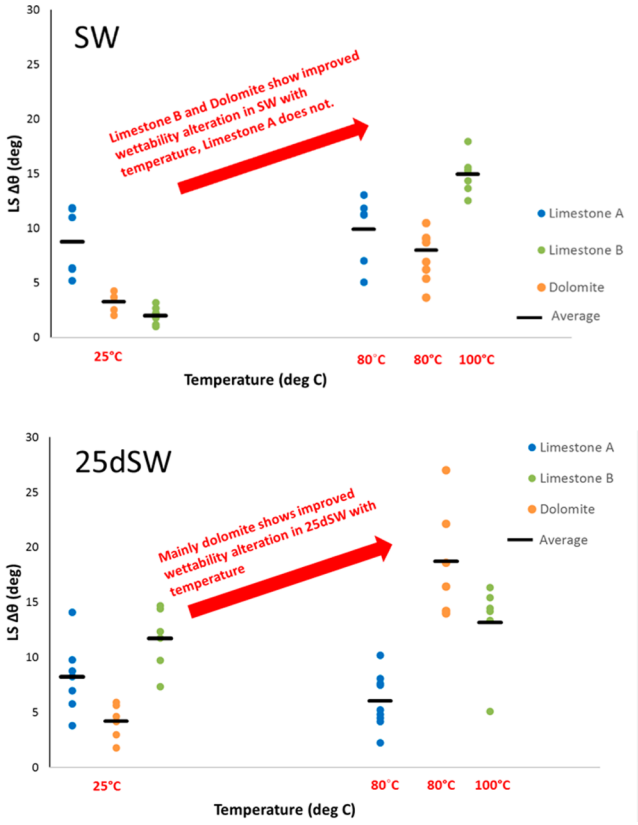

Figure 2. Contact angle change ($\Delta\theta$) with temperature for two limestone and one dolomite rock types. Each dot represents a different oil droplet (either in SW or in 25dSW), and the horizontal black bars indicate the average value of the contact angle change for all droplets at a particular temperature for each respective rock type.

against the initial contact angle. This can be seen later in Figure 3A, B for one of the cases studied.

Details of the contact angle changes for each rock in SW and 25dSW at ambient and elevated reservoir temperatures are summarized in Table 4. As can be seen, the typical range of contact angle changes observed at elevated temperatures in all samples varies between 7° and 18° on average for similar exposure times to SW and 25dSW brine. Moreover, the results reveal that both 25dSW and SW are effective at elevated temperature. This is a good indication that having large quantities of PDIs is not necessary and dilution of a brine can be suitable as well.

To illustrate the difference in contact angle data for SW at ambient and elevated temperatures in a more visual way, we take the Limestone B as an example. Figure 3 provides details of the contact angle data versus time at 25 and 100 °C.

Effect of Salinity and pH on ζ-Potential. In this section, the ζ-potential results for respective rocks and brines (HS and LS) at varying temperatures are presented and discussed to understand the reasons behind the contact angle results.

Figure 4 represents the results obtained for Limestone A and Crude oil A using 4 brines (FW, SW, 25dSW, and NaCl) at 25 °C. In all the brines (FW, SW, and 25dSW) containing divalent ions, we observe a trend of increasing rock ζ-potential with pH (as reported in ref 20), which suggests that, at a higher pH range, we see a shift of potentials from a negative value toward a positive (in case of FW, a shift from less positive toward more positive). In the literature (see, for instance, refs 35−39), an

DOI: 10.1021/acs.energyfuels.7b00776
Energy Fuels 2017, 31, 7839−7853

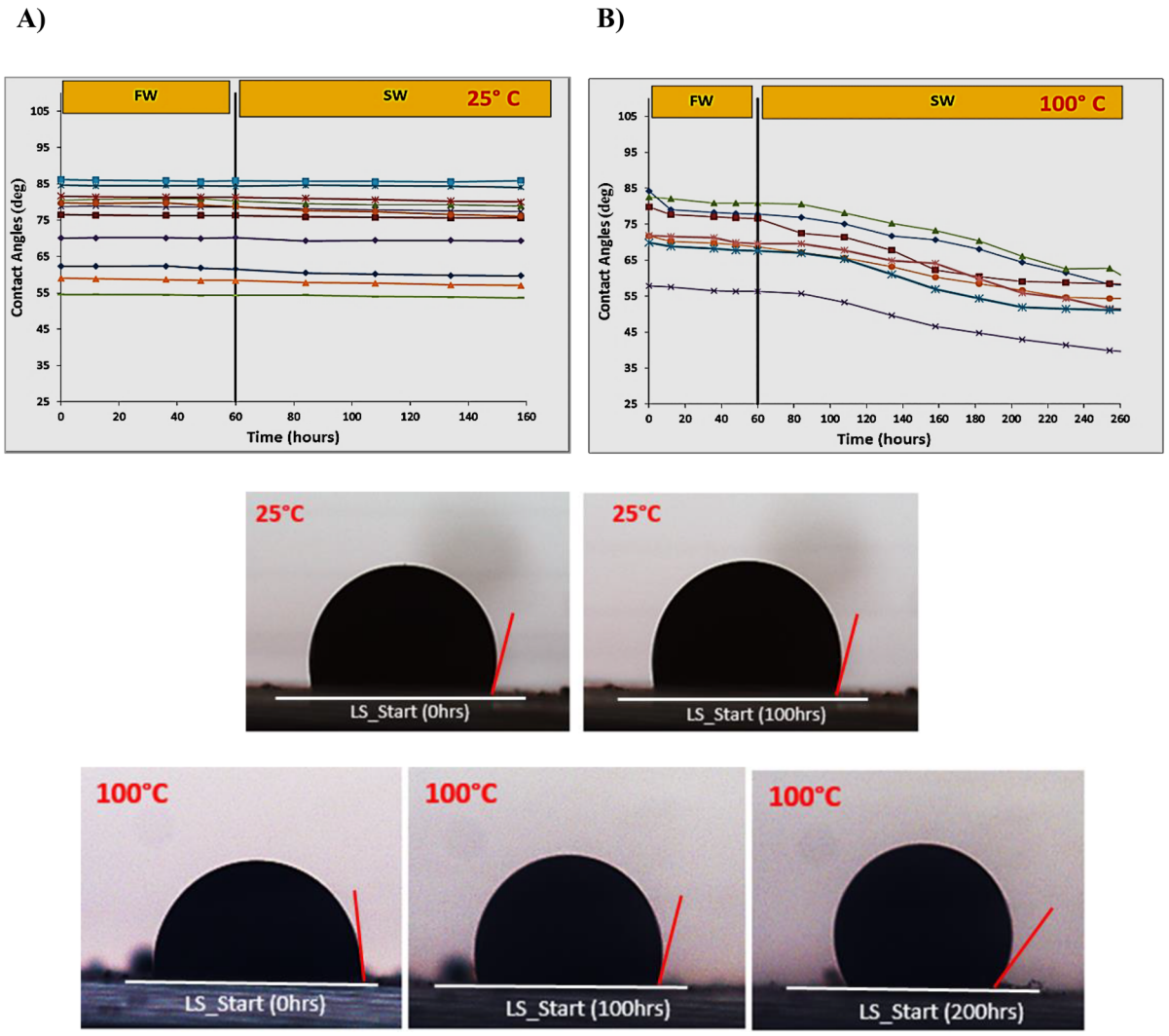

Figure 3. (Top) Contact angle change for Limestone B sample from FW to SW brine at (A) ambient temperature (25 °C) and (B) elevated temperature (100 °C). (Bottom) Oil-droplet images for each temperature at the start of exposure to SW (after equilibration with FW) and the end of exposure period in SW.

Table 4. Oil-Droplet (Contact Angle Measurements) Results for Each Rock/Brine Type at a Specific Temperature[a]

rock type	brine	temperature (°C)	average contact angle change (deg)
Limestone A	seawater (SW)	25	9
	43 731 ppm	80	10
	diluted seawater (25dSW)	25	8
	1750 ppm	80	7
Limestone B	seawater (SW)	25	2 (very minor) *
	43 731 ppm	100	15
	diluted seawater (25dSW)	25	12
	1750 ppm	100	13
Dolomite	seawater (SW)	25	3 (minor) *
	43 731 ppm	80	8
	diluted seawater (25dSW)	25	4 (minor) *
	1750 ppm	80	18.8

[a]The cases marked with (*) show very minor−minor contact angle change. Contact angle error (± 2°).

opposite trend with pH (i.e., the downward trend) has been mainly reported which one can expect with brines such as NaCl or KCl containing only monovalent, in-different ions. To demonstrate this, ζ-potential with pure NaCl brine (salinity = 2541 ppm) was recorded as shown in Figure 4. As proposed in ref 20, the influence of divalent ions causes this trend to reverse

DOI: 10.1021/acs.energyfuels.7b00776
Energy Fuels 2017, 31, 7839−7853

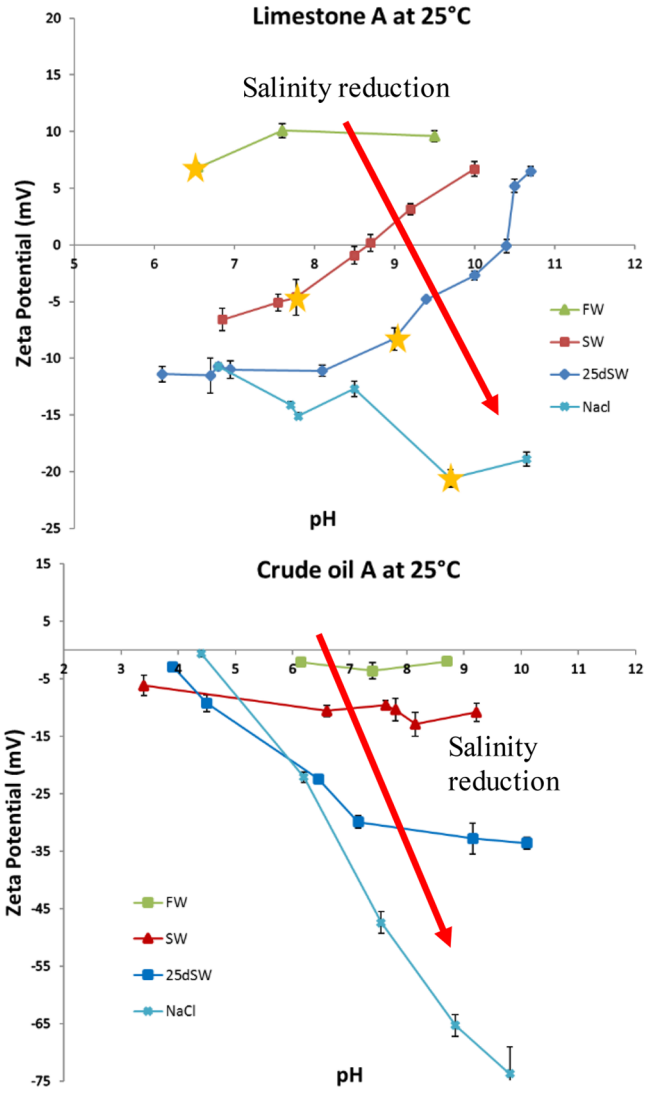

Figure 4. ζ-Potential for limestone A (Top) and Crude A (Bottom) as a function of pH and brine composition/salinity at ambient temperature (25 °C). The trend of ζ-potential with change in salinity is shown by the red arrows. The yellow stars indicate the equilibrated pH values of the sample in that respective brine.

due to their competition with H^+/OH^- for adsorption on the calcite surface and formation of surface complexes (denoted in the following with a ">"). At lower pH values (6–8), the surface concentration of the $>CaSO_4^-$ (complexes) are high, causing a negative charge on the rock surface. As pH is increased, the reaction reverses, causing a reduction in $>CaSO_4^-$ and increase in $>CaOH^0$, while $>CO_3Ca^+$ and $>CO_3Mg^+$ remain constant and are not affected much by pH; hence, the net charges on the surface become less negative/more positive and we observe an increase in ζ-potential with increase in pH.

Another important observation is the effect of salinity: as the salinity decreases from FW (>180 000 ppm) to 25dSW (1750 ppm), we observe a decrease in the ζ-potential toward more negative values. This can be explained by a double-layer expansion at a lower salinity, as well as more negative charges at the calcite surface due to the change in the concentration of surface complexes. However, the trend of increasing ζ-potential with pH is slightly more pronounced in the low salinity diluted brines; this can be observed with the increasing slope of the curve as we move down in salinity. The slope of ζ-potential in FW is fairly constant or very minor over the pH range measured—due to a compressed double layer. The isoelectric points (IEPs) decrease with increasing salinity.

The effect of salinity on the surface charges for Crude oil A is similar to what we observe in the rock samples. The ζ-potential decreases with decreasing brine salinity. However, the magnitude is much larger (more negative) and the trends with pH are different, showing a decrease in ζ-potential with increase in pH (especially with diluted brines), and as the salinity increases (SW and FW), the negative slope reduces and shifts to a slight increase with pH. Noteworthy is that the IEP values for all brines are almost nearing the same pH value (between 3 and 4). This possibly occurs due to the neutralization of the polar (acidic) groups at those pH values as they are similar to the pK_a values (~3–4) of the acidic groups (for instance, carboxylic acids[40]). The increase in negative charges observed with increasing pH in the oil ζ-potential data is likely due to the deprotonation of the carboxylic groups (see ref 41), which leads to a negative charge at the interface; however, for the HS brine, the slope is fairly constant due to excess positively charged divalent ions like Ca^{2+} and Mg^{2+}. Note that these effects are likely crude oil specific and cannot be easily translated to different crudes with different composition.

Provided that the reduction of ζ-potential upon change of salinity at both oil/brine and rock/brine interfaces is sufficient such that the adhesion force between oil and rock reduces or becomes repulsive as compared to HS FW, then a change of wettability to a less-oil-wetting state can be expected. This will be covered further in the next sections.

Effect of Temperature on ζ-Potential. The ζ-potentials measurements were restricted up to a maximum of 70 °C due to the limitations of the Zetasizer instrument. Nevertheless, these measurements give us a fair understanding of the ζ-potentials trends with increasing temperature. The observed trends for change in ζ-potential with pH and salinity remains the same at both ambient and elevated temperatures and for all the rock types, although the magnitude of the ζ-potential varies. This is illustrated in Figure 5 for Limestone A.

Figure 6 represents the variation of ζ-potential with temperature for all rock and oil samples. A clear trend stands out when increasing the temperature from 25 to 50 °C and 70 °C. As temperature increases, the ζ-potentials start to shift toward the point of zero potential, either from more positive to less positive values or from more negative to less negative values. This implies that the oil and rock surfaces tend to become weakly charged (neutral). This shift is more visible for the low salinity brine (25dSW) where we observe an increase of ζ-potential (toward less negative) with increasing temperature; at higher salinity (in FW and SW), a slight change in ζ-potential toward zero potential is observed.

The small magnitude of the ζ-potential change in FW and SW could be attributed to the thin (compressed) double layer which limits ion transfer into the double layer. Moreover, it can be related to the higher concentration of SO_4^{2-} present in the SW brine which tends to adsorb more on the carbonate surface at higher temperatures and hence lowers the ζ-potential slightly. The same trend is also observed in diluted SW and low salinity NaCl brine. This could be because of the lower concentration of the divalent anions like SO_4^{2-} in the diluted SW; more of the divalent cations such Ca^{2+} and Mg^{2+} can

DOI: 10.1021/acs.energyfuels.7b00776
Energy Fuels 2017, 31, 7839–7853

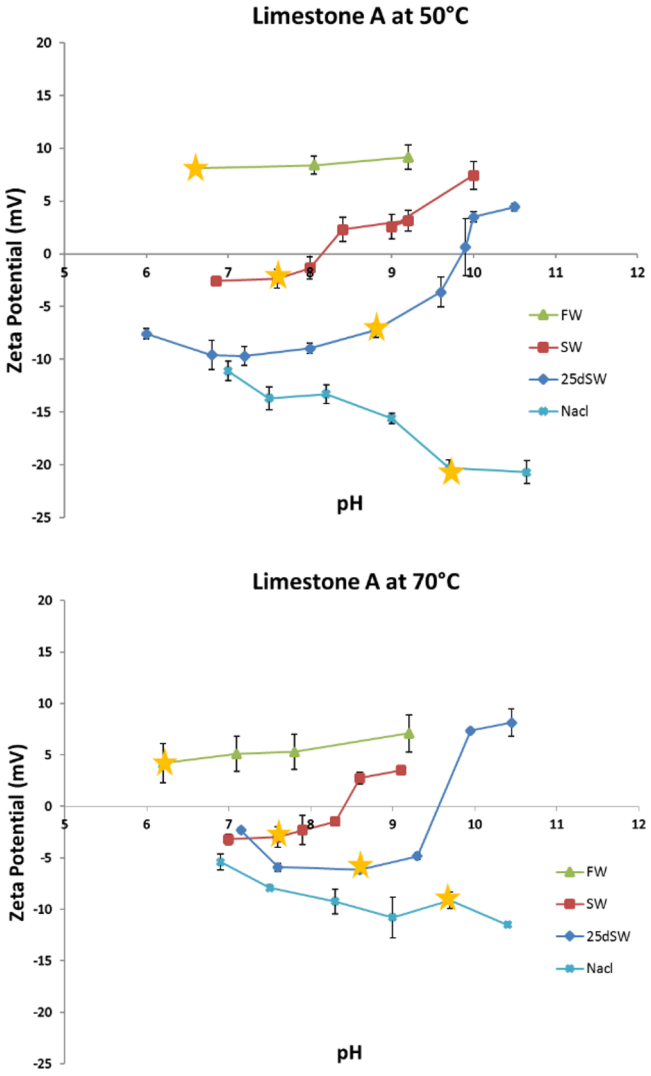

Figure 5. ζ-Potential for Limestone A as a function of pH and brine composition/salinity at 50 and 70 °C. The yellow stars indicate the equilibrated pH values of the sample in that respective brine.

adsorb onto the surface which can shift the ζ-potentials toward a less negative value. Al-Mahrouqi et al.[42] relate the decrease in the magnitude of ζ-potential to higher equilibrium calcium concentration (dissolution related) at higher temperature. Nevertheless, the observed trends with temperature (particularly for diluted brines) need to be evaluated further via developing a surface complexation model (SCM) for elevated temperature.

The crude oil (A and B) ζ-potentials remain negative throughout the temperature range, while their magnitude decreases at higher temperatures similar to that of the rocks. The reason for this trend remains to be fully understood. It is possible that it is somehow related to the increased interaction of divalent cations in the brine with the (negatively) charged polar groups of oil, which favors less negatively charged complexes at higher temperatures. To our knowledge, this is the first time that such ζ-potential behavior is reported.

ζ-Potential for Different Rock Types. While the ζ-potential trend with salinity and temperature holds for all the rock types, there are interesting differences between limestone and dolomite samples (refer to Figure 6). Both Limestone A and Limestone B show negative ζ-potential at lower salinity

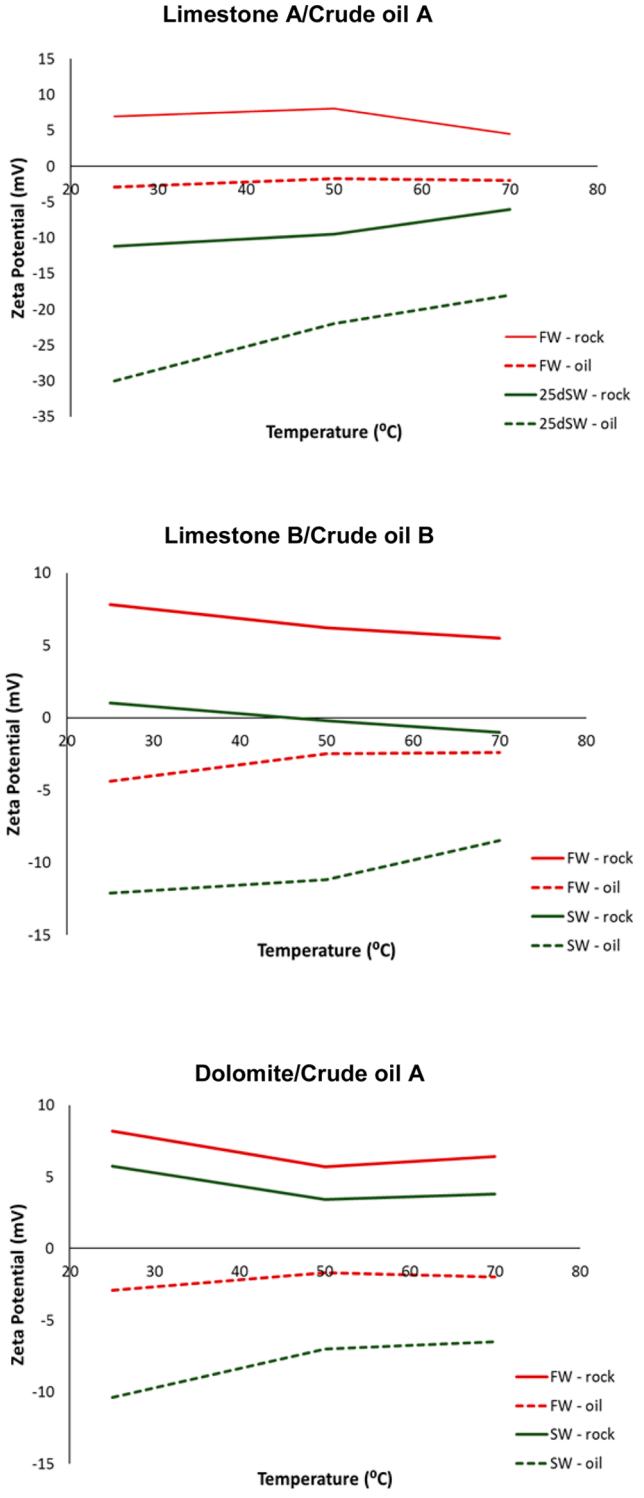

Figure 6. Effect of temperature on ζ-potential for Limestone A/Crude A (top), Limestone B/Crude B (middle), and Dolomite/Crude A (bottom) in selected brines, all at equilibrium pH with the brine of interest.

brines (25dSW, SW) which increase toward more positive at elevated temperatures (50, 70 °C). Dolomite, on the other hand, shows more positive ζ-potential in all brines at all temperatures. The difference between the magnitude of charge between limestones and dolomite was proposed (see ref 20) to be related to higher charge density on dolomite versus limestone due to the presence of Mg^{2+} in the composition of

DOI: 10.1021/acs.energyfuels.7b00776
Energy Fuels 2017, 31, 7839−7853

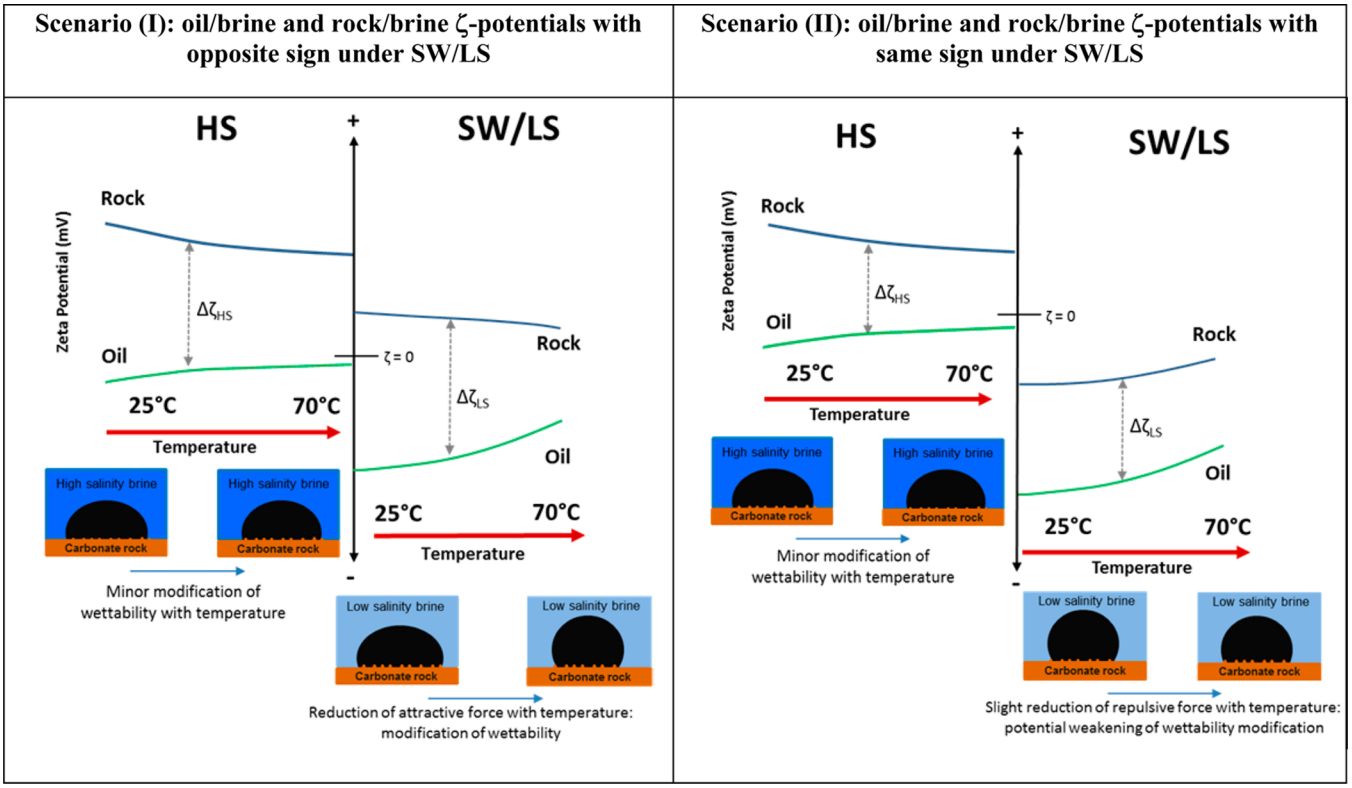

Figure 7. Schematic behavior of rock/brine and oil/brine ζ-potential as a function of temperature for two scenarios and its consequence on wettability alteration. The green and blue curves represent oil/brine and rock/brine ζ-potential, respectively: scenario (I) representing dolomite in SW/25dSW and Limestone B in SW, scenario (II) representing Limestone A under SW/25dSW and Limestone B under 25dSW.

the sample; i.e., dolomite is $CaMg(CO_3)_2$ while limestone contains mainly calcite, $CaCO_3$. This highlights the importance of rock type and mineralogy in the ζ-potential behavior.

Moreover, there is even a difference in behavior of Limestone A and B, both of which are composed of almost 100% calcite. The ζ-potential of Limestone A shows more pronounced reaction to change of salinity from FW to SW or 25dSW. This could be attributed to the possibility of having different grain structures and degree of crystallinity because of a different diagenetic history. The more crystalline the grain structure, the less reactive the surface would be, and the more amorphous the grain structure, the more reactive. This observation is in-line with the previous results in ref 20, where the crystalline limestone (Iceland spar calcite) showed a lesser potential (surface reactivity) in LS brine as compared to chalk (amorphous) which had the same mineralogical content but possibly different grain structure.

Interestingly, in all rock types, the difference between oil and rock ζ-potential ($\Delta\zeta = |\zeta_o - \zeta_r|$) under high salinity decreases slightly with temperature, indicating minor change of attractive electrostatic force between oil and rock, hence minor wettability alteration. It seems that $\Delta\zeta$ and the signs of ζ_o and ζ_r are good qualitative indicators for the response to LSF. This will become more evident from DLVO calculations in the next section. For all rocks and oils, ζ_o and ζ_r have opposite signs (negative and positive, respectively) under HS irrespective of temperature, indicating that electrostatic components of the surface forces are attractive—which promotes oil-wetness as expected. For Limestone A, ζ_o and ζ_r have the same signs (both negative) in SW and LS regardless of temperature. This means that the electrostatic forces are repulsive in low salinity, the magnitude of which slightly decreases with an increase of temperature. For Limestone B, again under LS condition, the force is repulsive at all temperatures; however, under SW at ambient condition, the rock exhibits a positive ζ-potential. Thus, electrostatic interactions are attractive—implying a weak tendency toward more oil-wetness. At higher temperatures, though, the behavior becomes similar to Limestone A. For dolomite, due to the opposite sign of ζ-potentials, the force remains attractive under both HS and LS, but under LS conditions, it becomes less attractive (based on $\Delta\zeta$ reduction) as the temperature increases, which is favorable for wettability alteration. This overall impact of salinity and temperature on ζ-potential of oil and rock samples is shown conceptually in Figure 7.

Analysis of DVLO Force under HS and LS Conditions. Already from ζ-potential data, we could observe some trends with salinity and temperature. However, following the ζ-potential concept, we have to consider separate trends for crude oil/brine and rock/brine interfaces and can only reason about the qualitative interaction. In order to integrate both individual ζ-potential measurements into one consistent concept for the forces present at the COBR interfaces, the results are presented in terms of the total interaction potential which accounts for the EDL and VDW interactionss as described in the section DLVO Interaction Force Calculation. For each COBR system we compare 25dSW and SW to the high salinity FW at a specific temperature.

It is important to mention that, in the oil-droplet experiments, once the carbonate patches have been deposited on the slide, oil is placed directly on the carbonate to enforce contact. However, since the carbonate patches are deposited by drying under environmental humidity (>20% humidity), the thin water layer remains present on the carbonate surface and

DOI: 10.1021/acs.energyfuels.7b00776
Energy Fuels 2017, 31, 7839−7853

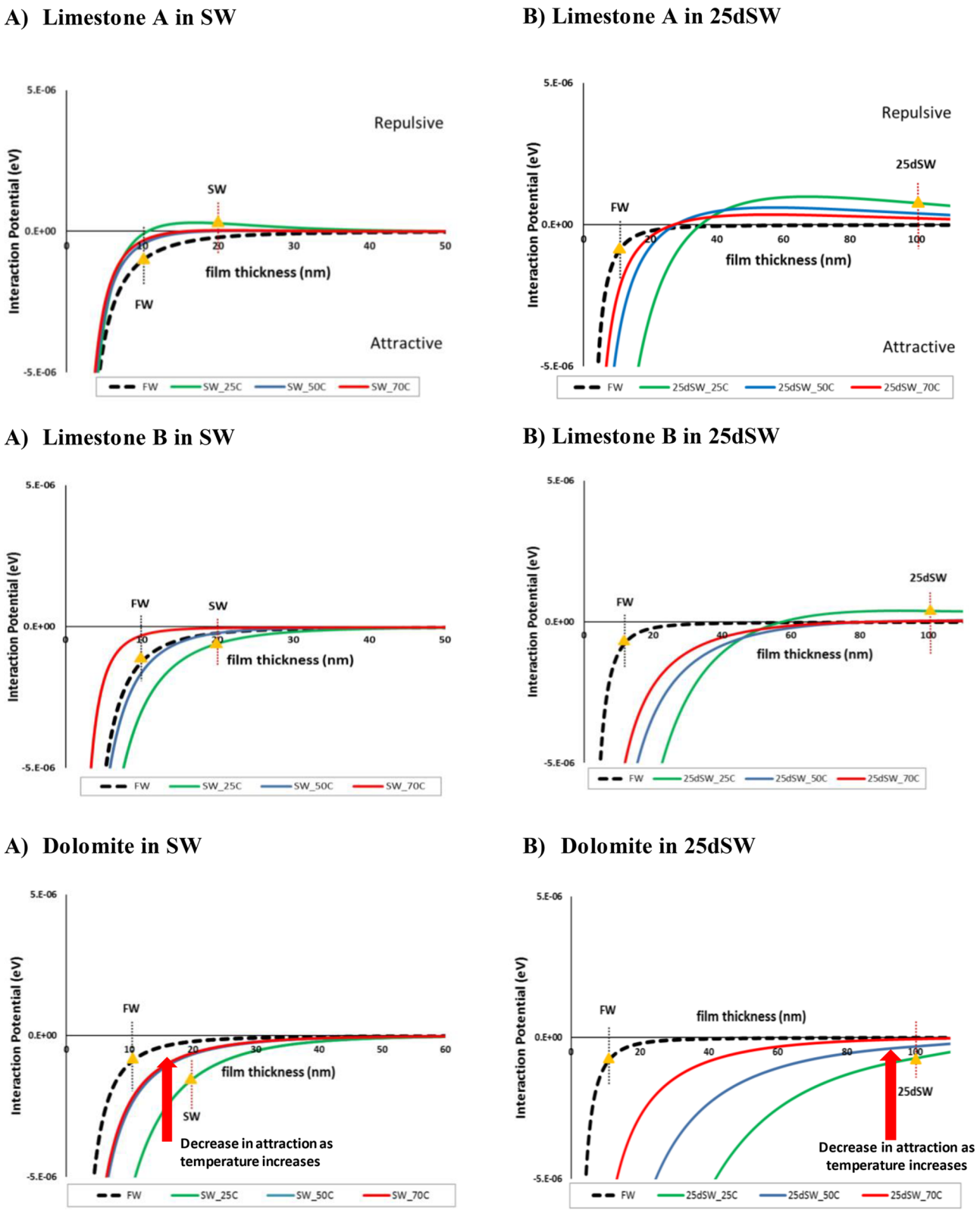

Figure 8. DLVO interaction potential from the measured ζ-potentials for HS and LS brines in Limestone A, Limestone B, and Dolomite at varying temperature. In each plot, green, blue, and red curves illustrate the interaction potentials at 25, 50, and 70 °C, respectively. The black and red dashed lines represent the equilibrium film thickness under FW and lower salinity (SW or 25dSW) conditions, respectively. The yellow triangles show the interaction potential at each salinity condition.

at the corners due to the capillary condensation of water. Therefore, the carbonate patches are, strictly speaking, "quasi-dry". Because of opposite sign of carbonate and oil ζ-potential, the film can collapse at points of direct contact of oil with carbonate such as sharp edges, but since the carbonate patch surface is rough (with the roughness height in order of

DOI: 10.1021/acs.energyfuels.7b00776
Energy Fuels 2017, 31, 7839−7853

Table 5. Comparison of the DLVO Prediction and the Oil-Droplet Results

sample	brine	temperature (°C)	contact angle change	DLVO prediction and oil-droplet results
Limestone A	SW	25	yes	consistent
	SW	80	yes	consistent
	25dSW	25	yes	consistent
	25dSW	80	yes	consistent
Limestone B	SW	25	very minor	consistent
	SW	100	yes	consistent (DLVO trend extrapolated to 100 °C)
	25dSW	25	yes	consistent
	25dSW	100	yes	consistent (DLVO trend extrapolated to 100 °C)
Dolomite	SW	25	minor	consistent
	SW	80	yes	consistent (DLVO trend extrapolated to 80 °C)
	25dSW	25	minor	consistent
	25dSW	80	yes	consistent (DLVO trend extrapolated to 80 °C)

nanometer to micrometer), the separation between oil and carbonate would limit the collapse of water film. This view is supported by previous experiments on clay/quartz substrate[28] and recent micromodel experiments.[1] It was observed that, after exposure of the oil saturated micromodel to high salinity brine, the water film (even though not present initially) starts forming and subsequently dewetting patterns at the solid−liquid interface appear. Concomitantly, the contact angle changes until reaching equilibrium. A similar process is thought to occur during the equilibration of oil droplets in HS which further develops during LS. Thus, it is realistic to consider the presence of water film beneath the oil as used in the DLVO calculation.

For the DLVO calculation, the ζ-potential data values for every specific brine are taken at the pH values corresponding to the oil-droplet experimental condition. For example, the original pH value of 25dSW is 7.5, but the pH value after equilibration with the Limestone A sample observed during the experiment is 8.9. Therefore, in the DLVO calculation, we have used the experimental equilibrated pH value of 8.9. The used ζ-potentials for each rock-brine or oil-brine system is presented in Table A-2.

In Figure 8, the results for the calculated DLVO interaction potential for all the three rock types are presented. The interaction potential has been estimated as a function of the separation "h". Since the DLVO curves in Figure 8 represent the equilibrium states under HS and LS salinity conditions, it is quite reasonable to compare the disjoining potential at equilibrium separation which is 2 × Debye screening length (k^{-1}) under each salinity condition. For each HS and LS case, the 2 × Debye length and the corresponding disjoining potential have been shown with yellow triangles. The calculated separations in FW, SW, and 25dSW using eq 7 are approximately 10, 20, and 100 nm, respectively. The variation of the Debye length with temperature is quite negligible for the temperature range studied.

In Figure 8, we observe that the DLVO potentials in FW are negative for all cases, which indicate a highly attractive force between the interfaces and an oil-wetting state in FW. Moreover, the potentials showed minor change with temperature, which, in terms of contact angles, would translate to no significant change with change of temperature alone. Therefore, we have only shown the data for 25 °C.

For Limestone A, the DLVO potentials in SW show an approximate constant range at all temperatures similar to FW; this is consistent with the ζ-potential data on the rock and oil interfaces we presented in the previous sections for the Limestone A samples (IEP values between 8.3 and 8.6). The 25dSW shows a large variation in DLVO potential with temperature, which is reflected in the ζ-potential data (IEPs decreasing from 10.5 to 9.5 with increasing temperature). However, in both brines, the potentials shift to a less positive/more negative value compared to the FW condition. This results in less attractive forces which enhances the wettability alteration toward a more water-wetting state.

Limestone B, as seen from the ζ-potential results as well, shows a more oil-wetting tendency in comparison to Limestone A. Although the ζ-potential values for all the brines fall within a close range of each other (approximately between +3 and −3 mV), we do observe the similar trends as Limestone A. In SW at 25 °C (the green curve), the potential is lower than the one in FW (the black curve) and reverses as the temperature increases to 70 °C (the red curve). On the basis of the contact angle results presented earlier, we do see that Limestone B shows a minor effect with SW at 25 °C while at 100 °C does show a larger effect; this behavior is quite consistent with the DLVO calculation. Note that the droplet experiments for Limestone B were carried out at 100 °C; however, the DLVO calculation could not be done at 100 °C due to the absence of ζ-potential data above 70 °C. Therefore, the DLVO trend with temperature was extrapolated.

Lastly, for Dolomite, which showed the least reactivity toward change of salinity and most positive ζ-potential values among all rocks, we observe a much larger variation of the DLVO potential with temperature. At ambient conditions, we observe that the potentials are much more negative for LS brines (the green curves) as compared to HS condition (the black curve). This can be understood from the sign and magnitude of the ζ-potentials of oil and dolomite. This means that it is not a given that, under LS brine, the double-layer forces become repulsive. It depends on the sign of the ζ-potentials. This is consistent with oil-droplet experiments which showed a minor change of contact angle in 25dSW and SW at 25 °C. However, as the temperature increases to 70 °C (the red curves), the potential becomes much less negative and closer to the HS condition. If we extrapolate the DLVO trend to 80 °C, at which the droplet experiments were conducted, we expect to see wettability modification due to reduction in the attractive forces between oil and dolomite.

Table 5 summarizes the above analysis, showing the overall consistency between the DLVO model and the droplet results.

Role of Oil-Brine IFT Change. To understand the role of IFT in wettability alteration, both the liquid-liquid (crude-brine) and the liquid-solid interfacial tensions have to be considered, as appear in Young's equation for contact angle.

DOI: 10.1021/acs.energyfuels.7b00776
Energy Fuels 2017, 31, 7839−7853

From Figure 9, we can observe that there is a slight reduction in IFT as the temperature increases; however, the IFT reduction is

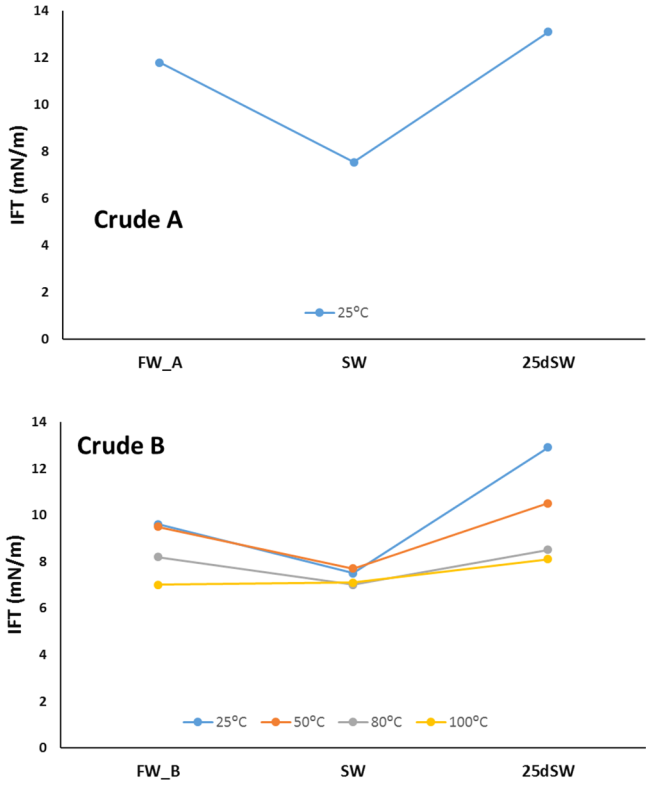

Figure 9. Crude oil-brine IFT measurements at varying temperatures. Measurement are at natural pH of brines. With increasing temperature, the IFT decreases slightly, and with decreasing salinity toward 25dSW, the IFT increases slightly. IFT in SW is comparatively lower than that in FW or 25dSW.

not significant. It is also observed that IFT goes through a minimum as salinity is decreased. IFT in SW is lower than that in FW which can have some contribution toward contact angle reduction. However, we observe an increase in the IFT for diluted SW which has a counter effect toward the observance of LSE in carbonates with this brine.

On the basis of Young's equation, a significant reduction in IFT by a factor of 2 or more in some cases is required to justify the observed contact angle changes in different brines. If the liquid-liquid surface forces were considered to be the driving force for the LSE, we would observe a similar contact angle change for Limestone A and Dolomite where the same brine and oil were used. Moreover, we would not observe an LSE in Limestone B at elevated temperatures because the IFT values at elevated temperatures are almost the same in all brines.

In addition to the above, it is worth mentioning that IFT is a function of both salinity and pH. pH of brine can change during the experiment due to chemical interaction with carbonate rock, which has an impact on IFT. In experiments under FW and SW, due to the absence of mineral dissolution, there was no measurable pH change and thus no anticipated change in IFT. In the experiments with limestones under 25dSW, there was a pH increase of ca. 1.4 due to calcite dissolution. As a result, the IFT at 25dSW was reduced by ca. 4 mN/m, which is almost equal to IFT at SW. This could have contributed in part to changes of contact angle, but it cannot be the dominant driving mechanism behind LSE, as a much more significant change of IFT is required to explain the changes of contact angle of all droplets. Also, in view of the fact that, for Limestone B at 25 °C, SW showed a very minor LSE while 25dSW did show a larger LSE, we have further evidence that IFT change to the level of SW either was insufficient (if IFT change is assumed to be the primary mechanism) or is not a primary mechanism. The former is in disagreement with the results for Limestone A in SW, where SW showed a clear LSE. For the case of dolomite under 25dSW, there was a minor pH increase of 0.1 because dissolution of dolomite is orders of magnitude less than calcite. Therefore, negligible IFT change due to pH change is expected.

The above-mentioned explanations suggest that the main driving force for this wettability alteration and LSE should be attributed to the change of solid-liquid surface energies rather than change of crude oil-brine IFT. Nevertheless, in case that IFT is decreased by the reduction of salinity, IFT change can be a contributing mechanism toward wettability alteration.

It's worth mentioning that investigating the role of interfacial rheology and viscoelasticity of crude/brine interface (see, e.g., refs 43 and 44) which can be mainly relevant during flow in a pore network, was not in the scope of the study; therefore, detailed study is suggested to substantiate their contribution in the LSF process.

Outlook. We do expect that a better (more accurate) DLVO prediction can be obtained by solving the PBE numerically, also in view of the fact that the CP-CP boundary condition has underestimated the DLVO potential. A following step would be using the DLVO model to estimate the intrinsic contact angles under high salinity and low salinity conditions and then compare it with the values from the experiments. This would then help to bridge the gap between the molecular scale interactions and the droplet scale contact angle. Moreover, the nonequilibrium effects meaning the transition of the system equilibrated in HS to the new equilibrium in LS could not be captured in the DLVO model, because it would require solving the PBE and other governing equations under dynamic conditions (see ref 45). This can be an interesting subject for future studies which can give insight into the kinetics of the process. Another aspect worth investigating in the future is the effect of longer aging time of oil droplets and carbonate patches on the studied process because the chemical interactions between oil functional groups and mineral surface are time-dependent and can affect the initial wettability.

SUMMARY AND CONCLUSIONS

The main objective of this study was to understand if the LSE (i.e., wettability alteration) truly depends on temperature and, if so, how does it change with temperature. Our findings have been summarized below:

- Contact angle response to LSF at elevated temperature.

By considering 3 different carbonate rocks (2 limestones, 1 dolomite), we did not observe a univocal increase in response to LSF at elevated temperature as outlined in the literature. The largest increase in contact angle response to LSF was observed for dolomite, while, for Limestone B only with SW and for Limestone A, no noticeable increase in LSF response was observed.

Moreover, the results reveal that both 25dSW and SW are effective at elevated temperature. This is a good indication that having large quantities of PDIs is not a necessity and dilution of a brine can be suitable as well.

- ζ-Potential as proxy for LSF response of rocks.

DOI: 10.1021/acs.energyfuels.7b00776
Energy Fuels 2017, 31, 7839−7853

All rock types showed a trend of contact angle response consistent with reduction in the ζ-potential. The ζ-potential showed a consistent trend toward more negative values with decreasing brine salinity at a specific temperature and an increase in ζ-potential with pH.

While there is a common trend in the ζ-potential response for all rocks, the magnitude of the ζ-potential exhibited a large sensitivity to rock type and mineralogy consistent with contact angle response in droplet experiments. Among the limestones, Limestone A showed more reactivity toward salinity change and more negative ζ-potential values as compared to Limestone B at the respective brine type.

Dolomite showed the most positive ζ-potential and the least reactivity toward low salinity in terms of change in ζ-potential values, which was again consistent with the contact angle data. The ζ-potentials were positive throughout the range of brines used and showed a decreasing ζ-potential in SW and diluted SW.

Furthermore, the ζ-potential values in all rock samples showed a similar behavioral trend with respect to temperature, showing a reduction of the ζ-potential magnitude toward zero potential. This was more visible in diluted brine than in FW and SW. However, the net effect on wetting behavior would depend on the ζ-potential of the oil/brine interface, sign of ζ-potentials, and the delta between the two potentials as captured in the DLVO model.

- DLVO prediction of low salinity response.

The DLVO calculation shows attractive forces (negative disjoining potential) between rock and crude oil in HS FW which translates to the tendency for oil-wetness as expected. Upon lowering salinity, we observed the trend of improving toward less attractive forces or increasing repulsion with an exception to dolomite, which did not alter much at lower temperature. However, at elevated temperatures, the disjoining potential showed a clear indication of improvement (toward less attractive) for the case of dolomite, some improvement for Limestone B under SW, and no major improvement for Limestone A. It is even observed that, for Limestone A, increased temperature may reduce the repulsive force, but still insignificant to be reflected in contact angle change. These observations matched the oil-droplet results well, which suggests that rock−fluid interactions (surface-charge change combined with double-layer expansion) rather than IFT change can be a plausible primary driving mechanism for LSF.

■ ASSOCIATED CONTENT

Supporting Information

The Supporting Information is available free of charge on the ACS Publications website at DOI: 10.1021/acs.energyfuels.7b00776.

Table A-1. Other input parameters to the DLVO model. Table A-2. The measured ζ-potentials at different temperatures and at pH corresponding to the oil-droplet experiments used as input to the DLVO model. (PDF)

■ AUTHOR INFORMATION

Corresponding Author

*E-mail: h.mahani@shell.com.

ORCID

H. Mahani: 0000-0002-3157-7991

Notes

The authors declare no competing financial interest.

■ ACKNOWLEDGMENTS

The authors thank Axel Makurat, the Rock and Fluid Science team leader, for providing support to execute this study. We thank Keschma Ganga, Ab Coorn, and Fons Marcelis for support in the experiments. We gratefully acknowledge Dr. Rouhi Farajzadeh for his detailed comments on the paper, and Shell Global Solutions International B.V. for permission to publish this work.

■ REFERENCES

(1) Bartels, W.-B.; Mahani, H.; Berg, S.; Menezes, R.; van der Hoeven, J. A.; Fadili, A. Oil Configuration Under High-Salinity and Low-Salinity Conditions at Pore Scale: A Parametric Investigation by Use of a Single-Channel Micromodel. *SPE J.* **2017**, SPE-181386-PA.

(2) Ligthelm, D. J.; Gronsveld, J.; Hofman, J. P.; Brussee, N. J.; Marcelis, F.; van der Linde, H. Novel Waterflooding Strategy by Manipulation of Injection Brine Composition. In *EUROPEC/EAGE Conference and Exhibition*, Amsterdam, The Netherlands, June 8−11, 2009; EAGE: Houten, The Netherlands, 2009; Paper SPE 119835.

(3) Morrow, N. R.; Buckley, J. Improved Oil Recovery by Low-Salinity Waterflooding. *JPT, J. Pet. Technol.* **2011**, *63*, SPE-129421-JPT.

(4) Jackson, M. D.; Vinogradov, J.; Hamon, G.; Chamerois, M. Evidence, mechanisms and improved understanding of controlled salinity waterflooding part 1: Sandstones. *Fuel* **2016**, *185* (2016), 772−793.

(5) Alotaibi, M. B.; Nasralla, R. A.; Nasr-EL-Din, H. A. Wettability Challenges in Carbonate Reservoirs. In *SPE Improved Oil Recovery Symposium*,Tulsa, OK, April 24−28, 2010; SPE: Richardson, TX, 2010; Paper SPE 129972.

(6) Yousef, A. A.; Al-Saleh, S.; Al-Kaabi, A.; Al-Jawfi, M. Laboratory Investigation of the Impact of Injection-Water Salinity and Ionic Content on Oil Recovery from Carbonate Reservoirs. *SPE Reservoir Eval. Eng. J.* **2011**, *14* (5), 578−593.

(7) Romanuka, J.; Hofman, J.; Ligthelm, D. J.; Suijkerbuijk, B. M. J. M.; Marcelis, A. H. M.; Oedai, S.; Brussee, N. J.; Van der Linde, H. A.; Aksulu, H.; Austad, T. Low Salinity EOR in Carbonates. In *SPE Improved Oil Recovery Symposium*, Tulsa, OK, April 14−18, 2012; SPE: Richardson, TX, 2012; Paper SPE 153869.

(8) Al Harrasi, A.; Al-maamari, R. S.; Masalmeh, S. K. Laboratory Investigation of Low Salinity Waterflooding for Carbonate Reservoirs. *Society of Petroleum Engineers* **2012**.

(9) Chandrasekhar, S.; Mohanty, K. K. Wettability Alteration with Brine Composition in High Temperature Carbonate Reservoirs. In *SPE Annual Technical Conference and Exhibition*, New Orleans, LA, Sept 30−Oct, 2, 2013; SPE: Richardson, TX, 2013; Paper SPE 166280.

(10) Alameri, W.; Teklu, T. W.; Graves, R. M.; Kazemi, H.; AlSumaiti, A. M. Wettability Alteration During Low-Salinity Waterflooding in Carbonate Reservoir Cores. In *SPE Asia Pacific Oil & Gas Conference and Exhibition*, Adelaide, Australia, Oct 14−16, 2014; SPE: Richardson, TX, 2014; Paper SPE-171529.

(11) Nasralla, R. A.; van der Linde, H.; Marcelis, F.; Mahani, H.; Masalmeh, S. K.; Sergienko, E.; Brussee, N.; Pieterse, S.; Basu, S. Low Salinity Waterflooding for a carbonate reservoir: Experimental evaluation and numerical interpretation. In *ADIPEC: The Abu Dhabi International Petroleum Exhibition & Conference*, Abu Dhabi, UAE, Nov 7−10, 2016; SPE: Richardson, TX, 2016; Paper SPE 183086.

(12) Sohal, M. A. N.; Thyne, G.; Søgaard, E. G. A Review of Recovery Mechanisms of Ionically Modified Waterflood in Carbonate Reservoirs. *Energy Fuels* **2016**, *30* (3), 1904−1914.

(13) Austad, T.; Strand, S.; Høgnesen, E. J.; Zhang, P. Seawater as IOR Fluid in Fractured Chalk. In *SPE International Symposium on Oilfield Chemistry*, The Woodlands, Texas, Feb 2−4, 2005; SPE: Richardson, TX; 2005; Paper SPE 93000.

(14) Strand, S.; Høgnesen, E. J.; Austad, T. Wettability Alteration of Carbonates − Effects of Potential Determining Ions (Ca^{2+} and SO_4^{2-}) and temperature. *Colloids Surf., A* **2006**, *275* (1−3), 1−10.

DOI: 10.1021/acs.energyfuels.7b00776
Energy Fuels 2017, 31, 7839−7853

(15) Hiorth, A.; Cathles, L.; Madland, M. The Impact of Pore Water Chemistry on Carbonate Surface Charge and Oil Wettability. *Transp. Porous Media* **2010**, *85* (1), 1−21.
(16) Nasralla, R. A.; Snippe, J. R.; Farajzadeh, R. Coupled Geochemical-Reservoir Model to Understand the Interaction between Low Salinity Brines and Carbonate Rock. In *SPE Enhanced Oil Recovery Conference*, Kuala Lumpur, Malaysia, Aug 11−13, 2015; SPE: Richardson, TX, 2015; Paper SPE 174661.
(17) Mahani, H.; Keya, A.; Berg, S.; Bartels, W.-B.; Nasralla, R.; Rossen, W. Insights into the Mechanism of Wettability Alteration by Low Salinity Waterflooding (LSF) in Carbonates. *Energy Fuels* **2015**, *29* (3), 1352−1367.
(18) Rezaei Gomari, K. A.; Karoussi, O.; Hamouda, A. Mechanistic Study of Interaction Between Water and Carbonate Rocks for Enhancing Oil Recovery. In *SPE Europec/EAGE Annual Conference and Exhibition*, Vienna, Austria, June 12−15, 2006; SPE: Richardson, TX, 2006; Paper SPE 99628.
(19) Zhang, P.; Austad, T. Wettability and Oil Recovery from Carbonates: Effects of Temperature and Potential Determining Ions. *Colloids Surf., A* **2006**, *279*, 179−187.
(20) Mahani, H.; Keya, A. L.; Berg, S.; Nasralla, R. Electrokinetics of Carbonate/Brine Interface in Low-Salinity Waterflooding: Effect of Brine Salinity, Composition, Rock Type, and pH on Zeta-Potential and a Surface-Complexation Model. *SPE J.* **2017**, *22* (01), SPE-181745-PA.
(21) Hamouda, A. A.; Karoussi, O. Effect of Temperature, Wettability and Relative Permeability on Oil Recovery from Oil-wet Chalk. *Energies* **2008**, *1* (1), 19−34.
(22) Hamouda, A. A.; Rezaei Gomari, K. A. Influence of Temperature on Wettability Alteration of Carbonate Reservoirs. In *SPE/DOE Symposium on Improved Oil Recovery*, Tulsa, OK, April 22−26, 2006; Society of Petroleum Engineers: Richardson, TX, 2006; SPE-99848-MS. DOI: 10.2118/99848-MS.
(23) Tweheyo, M. T.; Zhang, P.; Austad, T. The Effects of Temperature and Potential Determining Ions Present in Seawater in Oil Recovery from Fractured Carbonates. In *SPE Improved Oil Recovery Symposium*, Tulsa, OK, April 22−26, 2006; SPE: Richardson, TX, 2006; SPE 99438.
(24) RezaeiDoust, A.; Puntervold, T.; Strand, S.; Austad, T. Smart Water as Wettability Modifier in Carbonate and Sandstone: A Discussion of Similarities/Differences in the Chemical Mechanisms. *Energy Fuels* **2009**, *23*, 4479−4485.
(25) Shariatpanahi, S. F.; Strand, S.; Austad, T. Evaluation of Water-Based Enhanced Oil Recovery (EOR) by Wettability Alteration in a Low-Permeable Fractured Limestone Oil Reservoir. *Energy Fuels* **2010**, *24* (11), 5997−6008.
(26) Yousef, A. A.; Al-Saleh, S.; Al-Kaabi, A. U.; Al-Jawfi, M. S. Laboratory Investigation of Novel Oil Recovery Method for Carbonate Reservoirs. In *Canadian Unconventional Resources and International Petroleum Conference*, Calgary, Alberta, Canada, Oct 19−21, 2010; SPE: Richardson, TX, 2010; Paper SPE 137634. DOI: 10.2118/137634-MS.
(27) Berg, S.; Cense, A. W.; Jansen, E.; Bakker, K. Direct Experimental Evidence of Wettability Modification by Low Salinity. *Petrophysics* **2010**, *51*, 314−322.
(28) Mahani, H.; Berg, S.; Ilic, D.; Bartels, W.-B.; Joekar-Niasar, V. Kinetics of Low-salinity-flooding Effect. *SPE Journal* **2015**, *20* (1), 008−020.
(29) Hunter, R. J. *Zeta-Potential in Colloids Science*; Academic Press: New York, 1981.
(30) Israelachivili, J. *Intermolecular and Surface Forces*; Academic Press: New York, 1993.
(31) Kar, G.; Chander, S.; Mika, T. The potential energy of interaction between dissimilar electrical double layers. *J. Colloid Interface Sci.* **1973**, *44*, 347−355.
(32) McCormack, D.; Carnie, S. L.; Chan, D. Y. C. Calculations of electric double-layer force and interaction free energy between dissimilar surfaces. *J. Colloid Interface Sci.* **1995**, *169*, 177−196.
(33) Sadeqi-Moqadam, M.; Riahi, S.; Bahramian, A. An investigation into the electrical behavior of oil/water/reservoir rock interfaces: The implication for improvement in wettability prediction. *Colloids Surf., A* **2016**, *490*, 268−282.
(34) Gregory, J. Interaction of unequal double layers at constant charge. *J. Colloid Interface Sci.* **1975**, *51*, 44−51.
(35) Van Cappellen, P.; Charlet, L.; Stumm, W.; Wersin, P. A Surface Complexation Model of the Carbonate Mineral-Aqueous Solution Interface. *Geochim. Cosmochim. Acta* **1993**, *57*, 3505−3518.
(36) Pokrovsky, O. S.; Schott, J.; Thomas, F. Dolomite Surface Speciation and Reactivity in Aquatic Systems. *Geochim. Cosmochim. Acta* **1999**, *63*, 3133−3143.
(37) Mielczarski, J. A.; Schott, J.; Pokrovsky, O. S. Surface Speciation of Dolomite and Calcite in Aqueous Solutions. In *Encyclopedia of Surface and Colloid Science*, 2nd ed.; Somasundaran, P., Ed.; Taylor & Francis: Boca Raton, FL, 2006; Vol. *8*, pp 5965−5978.
(38) Wolthers, M.; Charlet, L.; Van Cappellen, P. The Surface Chemistry of Divalent Metal Carbonate Minerals, a Critical Assessment of Surface Charge and Potential Data Using the Charge Distribution Multi-Site Ion Complexation Model. *Am. J. Sci.* **2008**, *308*, 905−941.
(39) Chilingar, G.; Haroun, M. *Electrokinetics for Petroleum and Environmental Engineers*; Wiley Publishers: Hoboken, NJ, 2015.
(40) Schüürmann, G.; Cossi, M.; Barone, V.; Tomasi, J. Predication of the pKa of carboxylic acids using the ab initio continuum-solvation model PCM-UAHF. *J. Phys. Chem. A* **1998**, *102* (33), 6706−6712.
(41) Arla, D.; Sinquin, A.; Palermo, T.; Hurtevent, C.; Graciaa, A.; Dicharry, C. Influence of pH and Water Content on the Type and Stability of Acidic Crude Oil Emulsions. *Energy Fuels* **2007**, *21* (3), 1337−1342.
(42) Al-Mahrouqi; Vinogradov, J.; Jackson, M. Temperature dependence of the zeta potential in intact natural carbonates. *Geophys. Res. Lett.* **2016**, *43* (11), 578−587.
(43) Alvarado, V.; Garcia-Olvera, G.; Hoyer, P.; Lehmann, T. E. Impact of Polar Components on Crude Oil-Water Interfacial Film Formation: A Mechanisms for Low-Salinity Waterflooding. In *SPE Annual Technical Conference and Exhibition*, Amsterdam, The Netherlands, Oct 27−29, 2014; SPE: Richardson, TX, 2014; Paper SPE 170807. DOI: 10.2118/170807-MS.
(44) Chávez-Miyauchi, T. E.; Firoozabadi, A.; Fuller, G. G. Nonmonotonic Elasticity of the Crude Oil−Brine Interface in Relation to Improved Oil Recovery. *Langmuir* **2016**, *32* (9), 2192−2198.
(45) Joekar-Niasar, V.; Mahani, H. Nonmonotonic Pressure Field Induced by Ionic Diffusion in thin Films. *Ind. Eng. Chem. Res.* **2016**, *55* (21), 6227−6235.

NOTE ADDED AFTER ASAP PUBLICATION

This article published July 25, 2017 with an error in the fourth paragraph of the Effect of Salinity and pH on ζ-Potential section. The corrected version published July 27, 2017.

DOI: 10.1021/acs.energyfuels.7b00776
Energy Fuels 2017, 31, 7839−7853